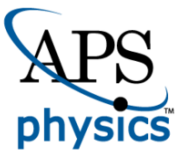

Separation of Time Scales in a Quantum Newton's Cradle

R. van den Berg, B. Wouters, S. Eliëns, J. De Nardis, R. M. Konik, and J.-S. Caux

Phys. Rev. Lett. **116**, 225302 — Published 1 June 2016

DOI: 10.1103/PhysRevLett.116.225302

Separation of Timescales in a Quantum Newton's Cradle

R. van den Berg,[1] B. Wouters,[1] S. Eliëns,[1] J. De Nardis,[1] R.M. Konik,[2] and J.-S. Caux[1,*]

[1] *Institute for Theoretical Physics, University of Amsterdam, Science Park 904, 1098 XH Amsterdam, The Netherlands*

[2] *CMPMS Dept. Bldg 734 Brookhaven National Laboratory, Upton NY 11973, USA*

(Dated: May 6, 2016)

We provide detailed modeling of the Bragg pulse used in quantum Newton's cradle-like settings or in Bragg spectroscopy experiments for strongly repulsive bosons in one dimension. We reconstruct the post-pulse time evolution and study the time-dependent local density profile and momentum distribution by a combination of exact techniques. We furthermore provide a variety of results for finite interaction strengths using a time-dependent Hartree-Fock analysis and bosonization-refermionization techniques. Our results display a clear separation of timescales between rapid and trap-insensitive relaxation immediately after the pulse, followed by slow in-trap periodic behaviour.

The study of many-body quantum physics has recently been transformed by progress achieved in experiments on ultracold atoms [1]. The context of one-dimensional (1D) bosonic gases provides a particularly fertile ground for investigating physics beyond traditional paradigms [2], with concepts such as Luttinger liquids and integrability [3] playing a primary role.

One of the main probes of cold gases is Bragg spectroscopy [4–6], which consists in applying a pulsed monochromatic laser grating onto the gas, thereby creating excitations at (multiples of) the recoil momentum q. In [7, 8], a two-pulse sequence was optimized to populate the first $\pm q$ momentum satellites of a Bose-Einstein condensate. The theoretical description of this sequence relied on a two-state model where many-body dynamics were not included. In 1D however, many-body effects are inescapable. One of the fundamental models in this context is the Lieb-Liniger gas [9] of δ-interacting bosons. This model is relevant to the description of experiments [10], most prominently the quantum Newton's cradle experiment [11], in which a Bragg pulse is used to initiate oscillations. Bragg spectroscopy has also recently been used to investigate correlated 1D Bose gases of rubidium [12] and cesium [13], where heating resulting from the Bragg pulse was measured and matched using linear response in the Lieb-Liniger gas [14].

Our main objective is to model the effects of Bragg pulses for strongly correlated 1D Bose gases, from first principles, without approximation (so beyond linear response), for experimentally relevant setups. We study instantaneous pulses of varying amplitude A and wavevector q via their effect on physical observables: the time-dependent local density of the gas, and the experimentally more accessible momentum distribution function (MDF). We will first focus on the Tonks-Girardeau limit [15–17] of hard-core bosons both on a periodic interval and in a harmonic trap [18–26], and then, significantly, study finite interaction effects.

Modelling Bragg pulses: We model a Bragg pulse as a one-body potential $V(x) = V_0\cos(qx)$ coupling to the density $\hat{\rho}(x) = \hat{\Psi}^\dagger(x)\hat{\Psi}(x)$, where the Bose fields obey the canonical equal-time commutation relations, $\left[\hat{\Psi}(x),\, \hat{\Psi}^\dagger(y)\right] = \delta(x-y)$. For a general Bragg pulse the gas is perturbed for a finite duration T_0. We will however consider the regime where the motion of the particles during the pulse can be neglected (the Raman-Nath limit), also known as a Kapitza-Dirac pulse [27, 28]. Taking the limit $T_0 \to 0$ while keeping $A = V_0T_0$ finite, the Bragg pulse operator $\hat{U}_B$ is given by

$$\hat{U}_B(q,A) = \exp\left(-iA\int dx\, \cos(qx)\hat{\Psi}^\dagger(x)\hat{\Psi}(x)\right), \quad (1)$$

where we have set $\hbar = 1$. The action of the instantaneous pulse on a ground state $|\psi_{\rm GS}\rangle$ generates the initial state of a quantum quench [29–31]. Typical experimental pulses [11–13, 32] correspond to Bragg momentum $q \sim 2\pi n$ and $A \sim 1$, where n is the mean density.

The post-pulse time evolution is driven by the Lieb-Liniger (LL) model of interacting bosons

$$H_{\rm LL} = -\sum_{i=1}^{N}\frac{1}{2m}\frac{\partial^2}{\partial x_i^2} + 2c\sum_{1\le i<j\le N}\delta(x_i - x_j), \quad (2)$$

either on a ring with periodic boundary conditions or in a harmonic trap with $V_{\rm trap}(x) = \frac{1}{2}m\omega^2x^2$. Throughout the paper, all data is produced with $m = 1$.

Hard-core limit: We start by considering the hard-core limit. In this limit the bosonic many-body wavefunction can be related through the Fermi-Bose (FB) mapping [16] to the many-body wavefunction of free fermions $\psi_B(\boldsymbol{x};t) = \prod_{1\le i<j\le N}\mathrm{sgn}(x_i - x_j)\psi_F(\boldsymbol{x};t)$, where $\boldsymbol{x} = \{x_j\}_{j=1}^N$ and $\psi_F(\boldsymbol{x};t)$ is the usual Slater determinant of the free single-particle (SP) wavefunctions, $\psi_F(\boldsymbol{x};t) = \det_N\left[\psi_j(x_i;t)\right]/\sqrt{N!}$. Following [19, 24, 26], the bosonic one-body density matrix and thus the MDF can be computed efficiently in terms of a single determinant involving the time-dependent fermionic SP states.

In the hard-core limit we will consider two geometries, a ring geometry with no external potential and an infinite line in the presence of a parabolic trap. For the former,

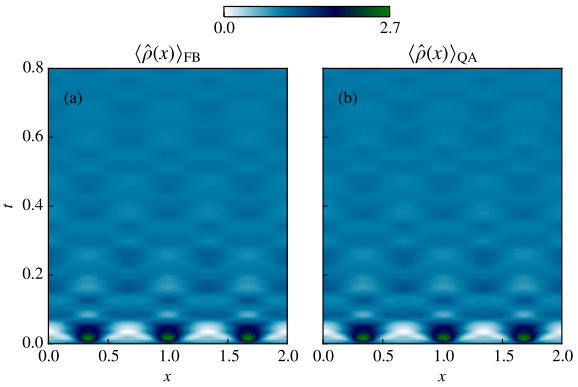

FIG. 1. Time evolution of the density after a Bragg pulse with $q = 3\pi$ and $A = 1.5$, computed by (a) the FB mapping and (b) the QA approach. The relative differences between the two results due to finite-size effects are less than 0.4%.

our ground state consists of SP plane waves, on which the Bragg pulse imprints a cosine phase due to the one-body potential,

$$\psi_j(x;t=0) = \frac{1}{\sqrt{L}} e^{-iA\cos(qx)} e^{-i\lambda_j^{\rm GS}x}, \tag{3}$$

with ground-state rapidities $\{\lambda_j^{\rm GS} = \frac{2\pi}{L}\left(-\frac{N+1}{2}+j\right)\}_{j=1}^{N}$ forming a Fermi sea with Fermi momentum $\lambda_F = \pi n$. Note that the Bragg momentum is quantized due to the periodic boundary conditions: $q = \frac{2\pi}{L} n_q$ with $n_q \in \mathbb{N}$. Expanding Eq. (3) in plane waves, the time-dependent SP wavefunctions after the Bragg pulse yield

$$\psi_j(x;t) = \sum_{\beta=-\infty}^{\infty} \frac{I_\beta(-iA)}{\sqrt{L}} e^{-i(\lambda_j+\beta q)x} e^{-i(\lambda_j+\beta q)^2 t/2m}, \tag{4}$$

with $I_\beta(z)$ the modified Bessel function of the first kind.

The Generalized Gibbs Ensemble (GGE) [30, 33] and the Quench Action (QA) approach [34, 35] enable the study of the Bragg pulsed system (on a ring) in the thermodynamic limit ($N \to \infty$ with N/L fixed). The GGE can be constructed using the infinite number of conserved charges $\{\hat{Q}_\alpha\}_{\alpha=1}^{\infty}$ provided by the integrability of the LL model, with $\hat{Q}_2 = 2m\hat{H}$, and eigenvalues $Q_\alpha(\boldsymbol{\lambda}) = \sum_{j=1}^{N} \lambda_j^\alpha$ associated to a Bethe state $|\boldsymbol{\lambda}\rangle = |\lambda_1, ..., \lambda_N\rangle$. The expectation values of the charges on the initial post-pulse state can be computed using the matrix elements for the Bragg pulse between two Bethe states $|\boldsymbol{\lambda}\rangle$ and $|\boldsymbol{\mu}\rangle$ [36], given by

$$\frac{\langle\boldsymbol{\mu}|\hat{U}_B(q,A)|\boldsymbol{\lambda}\rangle}{L^N} = \det_N\left[I_{\frac{\lambda_j-\mu_k}{q}}(-iA)\,\delta^{(q)}_{\lambda_j,\mu_k}\right], \tag{5}$$

where we defined $\delta^{(q)}_{\lambda,\mu} = \delta_{(\lambda-\mu)\bmod q,0}$. The GGE logic [30, 33] then requires the expectation values of all charges to be reproduced by the equilibrated post-pulse system, described by a density of rapidites $\rho^{\rm sp}_{q,A}(\lambda)$, i.e.

$$\lim_{\rm th} \frac{1}{L}\langle\psi_{q,A}|\,\hat{Q}_\alpha\,|\psi_{q,A}\rangle = \int_{-\infty}^{\infty} d\lambda\,\rho^{\rm sp}_{q,A}(\lambda)\,\lambda^\alpha\,, \tag{6}$$

for all $\alpha \in \mathbb{N}$. This leads to the stationary-state distribution [37][38]

$$\rho^{\rm sp}_{q,A}(\lambda) = \frac{1}{2\pi}\sum_{\beta\in\mathbb{Z}}\left[\theta(\lambda-\beta q+\lambda_F)-\theta(\lambda-\beta q-\lambda_F)\right]|I_\beta(iA)|^2 \tag{7}$$

where θ is the Heaviside step function. The saddle point distribution is a sum of copies of the ground-state density of rapidities, $\rho_{\rm GS}(\lambda) = \frac{1}{2\pi}\left[\theta(\lambda+\lambda_F)-\theta(\lambda-\lambda_F)\right]$, shifted by multiples of q and weighted by the modified Bessel functions. This form of the stationary state is consistent with the QA approach [39], which furthermore provides access to the time evolution of local observables by summing over particle-hole excitations in the vicinity of $\rho^{\rm sp}_{q,A}(\lambda)$ [34, 35, 40].

The time-dependent density of the hard core gas in the thermodynamic limit can be obtained via the QA approach or with the FB mapping. Interestingly, one can obtain the identical result from the non-interacting limit of the Tomonaga-Luttinger model with a quadratic band-curvature term. The non-linear Luttinger liquid theory (nLL) [41, 42] result for finite interactions reads [43]

$$\langle\hat{\rho}(x,t)\rangle = n + \sqrt{K}\sum_{\beta\neq0} J_\beta\left(-2\sqrt{K}A\sin\frac{\beta q^2 t}{2m^*}\right)\times \\ \times\cos(\beta qx)\frac{\sin(\beta q v_s t)}{\pi\beta q t/m^*}\,, \tag{8}$$

with $J_\beta(z)$ the Bessel function of the first kind. Here, K is the Luttinger parameter, v_s the sound velocity and m^* the renormalized effective mass. Surprisingly, the non-interacting limit with $K = 1$, $v_s = \lambda_F/m$, $m^* = m$, reproduces the exact TG result. The validity of Eq. (8) for finite interactions is discussed in the last section of this article. We compare the TG result against finite size FB computations for $N = 50$ in Fig. 1 and observe relative differences of the order of 0.4% due to finite-size effects. In the Raman-Nath limit, the post-pulse density at $t = 0$ is unaltered from the flat ground state profile. A sharp density profile then develops, mimicking the one-body cosine potential, followed by relaxation back to a flat profile at time scales $t \sim m/q\lambda_F = (qv_s)^{-1}$.

The QA approach also provides access to the time evolution of the MDF [44][45]. The result is plotted in Fig. 2 along with the FB result for $N = 50$. Except for minor disagreements in the sharp peaks due to finite-size effects, the large-system-size dynamics after the Bragg pulse is again well captured by a $N = 50$ FB mapping. At $t = 0$, one can show that the MDF (for any value

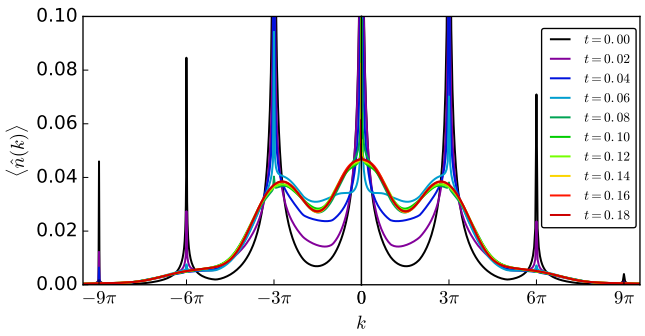

FIG. 2. Time evolution of the MDF after a Bragg pulse with $q = 3\pi$ and $A = 1.4$, computed with the QA approach (left half) and the FB mapping (right half). Because the FB mapping treats a finite system ($N = 50$) the momenta are quantized, causing less pronounced peaks for short times. All other results are in excellent agreement with the QA computations.

of c) is simply a sum of copies of the ground-state MDF [46], with a small-k divergence $\langle \hat{n}(k) \rangle_{\rm GS} \sim k^{-1/2}$ in the TG limit, centered around multiples of q. Similar to the initial MDF, the late-time distribution behaves like a superposition of independent peaks shifted to multiples of q, yielding a characteristic ghost-like shape [11]. The width of each satellite shows no dependence on the value of q, and is only influenced by the choice of A [47]. Since in the limit of $A \to 0$ the MDF reduces to the ground state time-independent distribution, the broadening can be ascribed to interactions between particles belonging to different satellites.

Next, we will use the FB mapping to investigate how these observations translate to the more experimentally relevant geometry of a harmonic trapping potential, with the Hamiltonian $H_{\rm trap} = H_{\rm LL} + \sum_{i=1}^{N} \frac{1}{2} m\omega^2 x_i^2$ and ω the trapping frequency. The ground state SP harmonic oscillator wavefunctions are given by

$$\psi_j(x) = \frac{1}{\sqrt{2^j j!}} \left(\frac{m\omega}{\pi}\right)^{1/4} e^{-\frac{m\omega x^2}{2}} H_j\left(\sqrt{m\omega}x\right), \qquad (9)$$

for $j = 1, ..., N$, with $H_j(x)$ denoting the Hermite polynomials. Using the propagator for the quantum harmonic oscillator [48], we compute the time evolution of the SP wavefunctions [49]:

$$\psi_j(x;t) = \sum_{\beta=-\infty}^{\infty} I_\beta(-iA) e^{-i\beta q \cos(\omega t)\left(x + \frac{\beta q}{2m\omega}\sin(\omega t)\right)} \psi_j(x + \tfrac{\beta q}{m\omega}\sin(\omega t)) e^{-i\omega(j+\frac{1}{2})t}. \qquad (10)$$

The SP wavefunctions are periodic in time with period $2\pi/\omega$, which is reflected in observables such as the density and the MDF. This periodicity is expected to be broken by finite-c interactions and anharmonicities in the trapping potential. The time evolution of the density and the MDF during one period is shown in Fig. 3, where the contributions from particles belonging to different satellites are clearly distinguishable. During the initial stages of relaxation (and around multiples of $t = \frac{\pi}{\omega}$) the density shows strong oscillations and the initially sharply peaked MDF relaxes rapidly to a broadened shape. This prerelaxation is well separated from the trap-induced collective periodic motion, suggesting that it is governed by the same physics as relaxation on a ring.

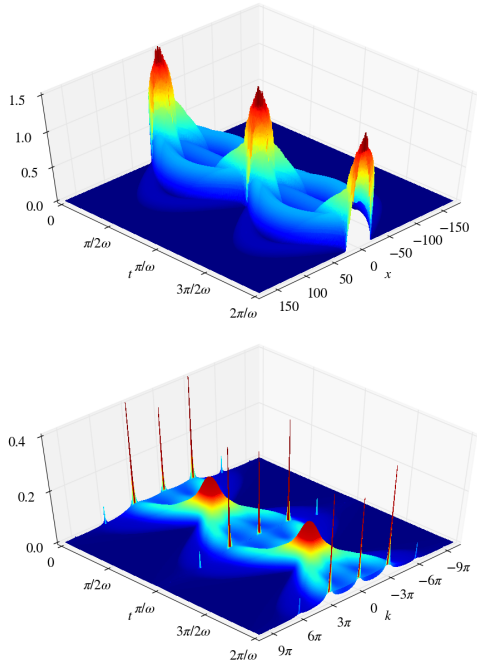

FIG. 3. The time evolution of the density (top) and MDF (bottom) in the trap, computed with the FB mapping for $N = 50$, $\omega = 10/N$, $A = 1.5$ and $q = 3\pi$.

In Fig. 4 the density at early stages in the oscillation cycle is compared to that on a ring, the latter being supplemented by a local density approximation (LDA) to account for the classical expansion of the gas in the trap [50] [51]. The initial density profile is accurately reproduced by the LDA, except for small differences near the edges originating from gradients in the local density not accounted for within the LDA [52–55]. Note however that these differences do not stay confined to the edges and propagate towards the center as time progresses.

The short-time MDF in the trap and ring geometry is shown in Fig. 5 up to $t = 0.015\pi/\omega$. The initial distributions are nearly identical, after which the MDFs dephase in a similar fashion to a (pre)relaxed ghost-like shape. The strong similarities can be attributed to the short-range correlations characterizing the post-quench steady state. Large-distance effects due to the trap geometry lead to discrepancies only at low momenta. The time scale associated to this (pre)relaxation is estimated to be the time it takes for a boson traveling with the speed of

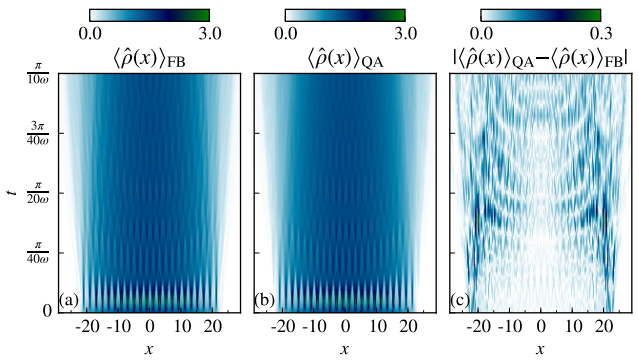

FIG. 4. Time evolution of the density in a trap, computed with: the FB mapping for $N = 50$ particles (a), the QA approach on a ring with an LDA accounting for the trap (b). The difference between the two results is shown in panel (c). The Bragg pulse parameters are set to $A = 1.5$ and $q = \pi$ with $\omega = 10/N$.

sound to traverse one density oscillation induced by the Bragg pulse: $t \sim 2\pi/qv_s$. Considering conditions similar to the Newton's cradle experiment, we estimate the short time scale to be of the order of 10 μs. This estimate is of the same order of magnitude as the pulse duration used in [11], suggesting that interaction effects can be important for longer pulses. This will be treated in future publications.

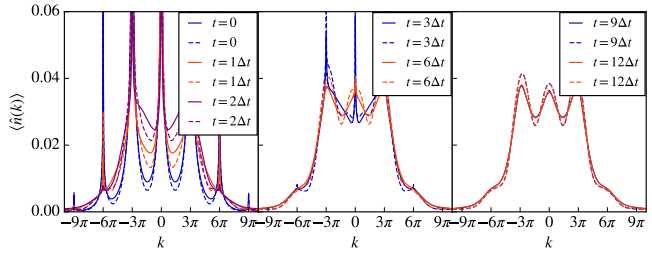

FIG. 5. Time evolution of the MDF for the trap geometry (solid lines) and the ring geometry (dashed lines), obtained with the FB mapping for $N = 50$ particles. The trapping frequency is set to $\omega = 10/N$, and we used $A = 1.5$ and $q = 3\pi$. The time step Δt is set to $\frac{\pi}{800\omega}$.

Finite interactions: We now extend our results to finite interactions by considering the dual fermionic model to Eq. (2) [56, 57][58]

$$H_{\rm F} = -\sum_{i=1}^{N} \frac{1}{2m}\frac{\partial^2}{\partial x_i^2} - \frac{1}{m^2 c}\sum_{1\le i<j\le N}\delta''(x_i - x_j). \quad (11)$$

Using a self-consistent time-dependent Hartree-Fock (TDHF) approximation [59, 60], we have performed finite-c calculations of the density and MDF, shown in panels (a), (c) and (d) of Fig. 6. The equilibrium Hartree-Fock computation yields an effective mass of the planewave quasiparticles given by $m^* = m/(1 - 2n/mc)$ [59, 60], suggesting that the the out-of-equilibrium finite-c results can be rescaled according to $t \to t(1 - 2n/mc)$, to produce the same time-dependent behaviour as in the $c \to \infty$ limit. This is confirmed by the rescaled results shown in panel (b). Furthermore, the density at $x = 0$ shows an enhancement of the high density regions for increasing c, consistent with a model for attractive fermions. The nLL result of Eq. (8) reproduces the correct time scaling for large values of c, but is unable to account for the increased density oscillations. This discrepancy can be attributed to the neglected irrelevant operators which cannot be justified by a renormalization group argument in out-of-equilibrium settings. In panel (c) the relaxation of the MDF at $k = 0, q, 2q$ shows a delay in relaxation consistent with a reduced sound velocity $v_s = \frac{\pi n}{m}\left(1 - \frac{2n}{mc} + \dots\right)$. Finally, the relaxed MDF in (d) depicts increasingly condensed satellites for smaller c, as is expected from bosons with decreasing repulsive interactions.

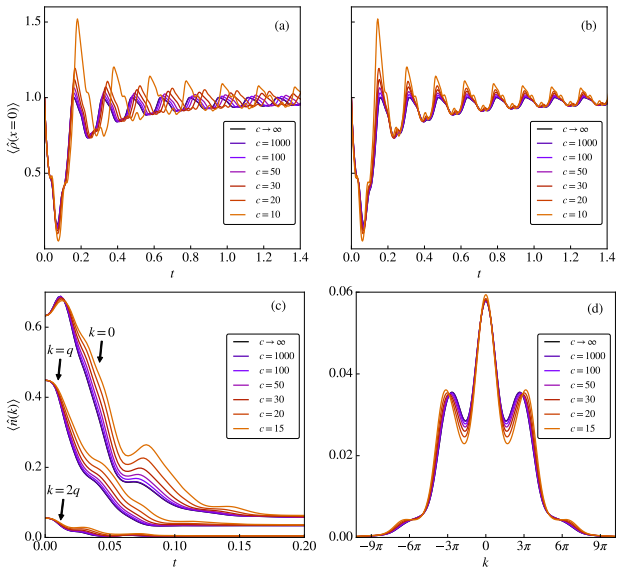

FIG. 6. Finite-c results using TDHF for the ring geometry. Time evolution of the density at $x = 0$ for $N = 50$, $A = 1$ and $q = 2\pi$ (a, b). In (b) the results of (a) are rescaled according to $t \to t(1 - 2n/mc)$. Time evolution of the MDF at $k = 0, q, 2q$ for $N = 50$, $A = 1.3$ and $q = 3\pi$ (c) and the relaxed MDF at $t = 0.4$ (d).

Conclusion: We have developed a theoretical description of the Bragg pulse for one-dimensional Bose gases and shown that the time evolution of physical observables for a Bragg pulsed Lieb-Liniger gas in a trap is characterized by two well-separated time scales. The shortest time scale is dominated by the trap-insensitive contact interactions and causes a substantial broadening of the momentum distribution well before the collective motion due to the presence of the trap sets in. Our work can be

extended to include finite interaction effects in harmonic traps [61], and opens up the possibility to study the influence of interactions on more general pulse protocols and to incorporate finite temperature effects.

We thank M. Brockmann, E.A. Demler, N.J. van Druten, V. Gritsev, F. Meinert, H.-C. Nägerl, J. Schmiedmayer, F.E. Schreck, D. Weiss and J. van Wezel for useful discussions. This work was supported by the Netherlands Organisation for Scientific Research (NWO) and the Foundation for Fundamental Research on Matter (FOM), and forms part of the activities of the Delta-Institute for Theoretical Physics (D-ITP). This research was done in part under the auspices of the CMPMS Dept. at Brookhaven National Laboratory, which in turn is supported by the U.S. Department of Energy, Office of Basic Energy Sciences, under Contract No. DE-AC02-98CH10886. We are grateful for support from the Centre de Recherches Mathématiques of the U. de Montréal.

* J.S.Caux@uva.nl

[1] I. Bloch, J. Dalibard, and W. Zwerger, Rev. Mod. Phys. **80**, 885 (2008).
[2] M. A. Cazalilla, R. Citro, T. Giamarchi, E. Orignac, and M. Rigol, Rev. Mod. Phys. **83**, 1405 (2011).
[3] T. Giamarchi, *Quantum Physics in One Dimension* (Oxford University Press, 2004).
[4] P. J. Martin, B. G. Oldaker, A. H. Miklich, and D. E. Pritchard, Phys. Rev. Lett. **60**, 515 (1988).
[5] J. Stenger, S. Inouye, A. P. Chikkatur, D. M. Stamper-Kurn, D. E. Pritchard, and W. Ketterle, Phys. Rev. Lett. **82**, 4569 (1999).
[6] R. Ozeri, N. Katz, J. Steinhauer, and N. Davidson, Rev. Mod. Phys. **77**, 187 (2005).
[7] Y.-J. Wang, D. Z. Anderson, V. M. Bright, E. A. Cornell, Q. Diot, T. Kishimoto, M. Prentiss, R. A. Saravanan, S. R. Segal, and S. Wu, Phys. Rev. Lett. **94**, 090405 (2005).
[8] S. Wu, Y.-J. Wang, Q. Diot, and M. Prentiss, Phys. Rev. A **71**, 043602 (2005).
[9] E. H. Lieb and W. Liniger, Phys. Rev. **130**, 1605 (1963).
[10] M. Olshanii, Phys. Rev. Lett. **81**, 938 (1998).
[11] T. Kinoshita, T. Wenger, and D. S. Weiss, Nature **440**, 900 (2006).
[12] N. Fabbri, M. Panfil, D. Clément, L. Fallani, M. Inguscio, C. Fort, and J.-S. Caux, Phys. Rev. A **91**, 043617 (2015).
[13] F. Meinert, M. Panfil, M. J. Mark, K. Lauber, J.-S. Caux, and H.-C. Nägerl, Phys. Rev. Lett. **115**, 085301 (2015).
[14] M. Panfil and J.-S. Caux, Phys. Rev. A **89**, 033605 (2014).
[15] L. Tonks, Phys. Rev. **50**, 955 (1936).
[16] M. Girardeau, J. Math. Phys. **1**, 516 (1960).
[17] E. Haller, M. Gustavsson, M. J. Mark, J. G. Danzl, R. Hart, G. Pupillo, and H.-C. Nägerl, Science **325**, 1224 (2009).
[18] A. Minguzzi and D. M. Gangardt, Phys. Rev. Lett. **94**, 240404 (2005).
[19] R. Pezer and H. Buljan, Phys. Rev. Lett. **98**, 240403 (2007).
[20] D. M. Gangardt and M. Pustilnik, Phys. Rev. A **77**, 041604 (2008).
[21] D. Muth, B. Schmidt, and M. Fleischhauer, New Journal of Physics **12**, 083065 (2010).
[22] C. Schenke, A. Minguzzi, and F. W. J. Hekking, Phys. Rev. A **84**, 053636 (2011).
[23] G. E. Astrakharchik and L. P. Pitaevskii, Europhys. Lett. **102**, 30004 (2013).
[24] M. Collura, S. Sotiriadis, and P. Calabrese, Phys. Rev. Lett. **110**, 245301 (2013).
[25] E. Quinn and M. Haque, Phys. Rev. A **90**, 053609 (2014).
[26] F. Cartarius, E. Kawasaki, and A. Minguzzi, arXiv:1505.01009.
[27] P. L. Kapitza and P. A. M. Dirac, Proceedings of the Cambridge Philosophical Society **29**, 297 (1933).
[28] D. L. Freimund, K. Aflatooni, and H. Batelaan, Nature **413**, 142 (2001).
[29] P. Calabrese and J. Cardy, Phys. Rev. Lett. **96**, 136801 (2006).
[30] M. Rigol, V. Dunjko, V. Yurovsky, and M. Olshanii, Phys. Rev. Lett. **98**, 050405 (2007).
[31] A. Polkovnikov, K. Sengupta, A. Silva, and M. Vengalattore, Rev. Mod. Phys. **83**, 863 (2011).
[32] R. E. Sapiro, R. Zhang, and G. Raithel, Phys. Rev. A **79**, 043630 (2009).
[33] M. Rigol, V. Dunjko, and M. Olshanii, Nature **452**, 854 (2008).
[34] J.-S. Caux and F. H. L. Essler, Phys. Rev. Lett. **110**, 257203 (2013).
[35] J. De Nardis, B. Wouters, M. Brockmann, and J.-S. Caux, Phys. Rev. A **89**, 033601 (2014).
[36] See section A in Supplemental Material.
[37] G. Bevilacqua, V. Biancalana, Y. Dancheva, T. Mansour, and L. Moi, J. Math. Phys. **52**, 033508 (2011).
[38] See section B in Supplemental Material.
[39] See section B in Supplemental Material.
[40] J. De Nardis, L. Piroli, and J.-S. Caux, arXiv:1505.03080.
[41] A. Imambekov and L. I. Glazman, **323**, 228 (2009).
[42] A. Imambekov, T. L. Schmidt, and L. I. Glazman, Rev. Mod. Phys. **84**, 1253 (2012).
[43] See section C in Supplemental Material, which includes Refs [62, 63].
[44] J. De Nardis and J.-S. Caux, J. Stat. Mech.: Th. Exp. **2014**, P12012 (2014).
[45] See section D in Supplemental Material.
[46] See section E in Supplemental Material.
[47] See section F in Supplemental Material.
[48] F. G. Mehler, J. Reine Angew. Math. **66**, 161 (1866).
[49] See section G in Supplemental Material.
[50] A. S. Campbell, D. M. Gangardt, and K. V. Kheruntsyan, Phys. Rev. Lett. **114**, 125302 (2015).
[51] See section H in Supplemental Material.
[52] K. V. Kheruntsyan, D. M. Gangardt, P. D. Drummond, and G. V. Shlyapnikov, Phys. Rev. A **71**, 053615 (2005).
[53] A. H. van Amerongen, J. J. P. van Es, P. Wicke, K. V. Kheruntsyan, and N. J. van Druten, Phys. Rev. Lett. **100**, 090402 (2008).
[54] J. Armijo, T. Jacqmin, K. Kheruntsyan, and I. Bouchoule, Phys. Rev. A **83**, 021605 (2011).
[55] T. Jacqmin, J. Armijo, T. Berrada, K. V. Kheruntsyan, and I. Bouchoule, Phys. Rev. Lett. **106**, 230405 (2011).
[56] T. Cheon and T. Shigehara, Phys. Rev. Lett. **82**, 2536 (1999).

[57] D. Sen, International Journal of Modern Physics A **14**, 1789 (1999).
[58] This form of the interaction potential is technically only correct for variational calculations such as Hartree-Fock approximations. For a more general form of the interaction potential valid for all orders of $1/c$ see section I in the Supplemental Material.
[59] J. Brand and A. Y. Cherny, Phys. Rev. A **72**, 033619 (2005).
[60] A. Y. Cherny and J. Brand, Phys. Rev. A **73**, 023612 (2006).
[61] M. Gattobigio, Journal of Physics B: Atomic, Molecular and Optical Physics **39**, S191 (2006).
[62] A. V. Rozhkov, Phys. Rev. B **77**, 125109 (2008).
[63] G. N. Watson, *A Treatise on the Theory of Bessel Functions*, 2nd ed. (Cambridge University Press, Cambridge, England, 1944) pp. vi+804, reprinted in 1995.